**COMMUNICATIONS IN SCIENCE AND TECHNOLOGY**
*Homepage:* cst.kipmi.or.id

# Fixing cobalt metal onto mordenite through spray impregnation and its evaluation as a catalyst in transforming used coconut cooking oil into bio-jet fuel

Aldino Javier Saviola[a], Karna Wijaya[a,*], Akhmad Syoufian[a], Marini Fairuz Vebryana[a], Widuri Anggraeni[a], Kharistya Rozana[a,b], Nono Darsono[c], Dita Adi Saputra[c], Wahyu Dita Saputri[d]

[a]*Department of Chemistry, Universitas Gadjah Mada, Yogyakarta 55281, Indonesia.*
[b]*Directorate of Laboratory Management, Research Facilities, and Science and Technology Park, National Research and Innovation Agency (BRIN), Yogyakarta 55281, Indonesia.*
[c]*Research Center for Energy Conversion and Conservation, National Research and Innovation Agency (BRIN), Banten 15314, Indonesia.*
[d]*Research Center for Climate and Atmosphere, National Research and Innovation Agency (BRIN), Bandung 40135, Indonesia.*

*Article history:*
Received: 15 September 2024 / Received in revised form: 4 November 2024 / Accepted: 9 December 2024

**Abstract**

Given the challenges posed by fossil-based jet fuel, research into bio-jet fuel production has intensified to achieve carbon neutrality. The present work reports a significant breakthrough with the successful conversion of used coconut cooking oil into bio-jet fuel utilizing a cobalt-impregnated mordenite catalyst. Cobalt was introduced to mordenite via the spray impregnation method at a concentration of 2% using a $CoCl_2 \cdot 6H_2O$ solution. The resultant catalyst was characterized using FTIR, XRD, $NH_3$-TPD, SAA, FESEM-EDX Mapping, TEM, XPS, and TG/DTA instruments. Hydrotreatment was conducted in a semi-batch reactor at atmospheric pressure, employing $H_2$ gas at a flow rate of 20 mL/min and a catalyst-to-feed ratio of 1:200 (w/w) for a duration of 2 h. The addition of cobalt significantly enhanced the efficiency of the hydrotreatment by improving the catalytic performance of mordenite as a support material. The liquid product conversion and total bio-jet fuel yield obtained from the hydrotreatment of used coconut cooking oil using the Co/mordenite catalyst were 60.25% and 51.11%, respectively. The highest selectivity for bio-jet fuel was observed in fraction II (450–550 °C) at 88.90%. This catalyst exhibited sustained performance over three consecutive runs, indicating its potential application in the future biofuel industry. Altogether, this research reveals the possibility of employing used coconut cooking oil as a sustainable and promising feedstock to be converted into bio-jet fuel by hydrodeoxygenation and/or hydrocracking reactions.

*Keywords:* Bio-jet fuel; cobalt; mordenite; used coconut cooking oil; hydrotreatment.

## 1. Introduction

The aviation industry, driven by the increasing demand for commercial and military air travel, is a significant contributor to the environmental crisis. Its heavy reliance on fossil fuels, coupled with projections indicating that the volume of passengers and cargo transported by air will double within the next two decades [1], underscores the urgency of the issue. The use of fossil fuel-based jet fuel is taking a heavy toll on the environment, with the aviation sector responsible for 2.5% of global $CO_2$ emissions as of 2018 [2]. As reported by Zhang et al. [3], carbon dioxide gas emissions will rise to 4% in 2050 if the airline industry's demand continues to increase year by year. This figure is set to rise unless the industry takes accountability and undertakes concerted efforts to reduce its usage, safeguarding the Earth's sustainability.

Consequently, there has been a burgeoning endeavor among stakeholders to diminish the excessive reliance on fossil fuels by exploring biofuels derived from the hydrotreatment process of biomass as a viable alternative. Bio-jet fuel not only enhances energy security and reduces greenhouse gas emissions but also contributes to achieving environmental equilibrium within the aviation sector [4,5]. Despite ongoing research into the blending of bio-jet fuel with conventional jet fuel and its global application, investigations into renewable resources for bio-jet fuel production persist. The importance of international standards for large-scale production cannot be overstated, highlighting the need for global cooperation in this crucial endeavor.

Several biomass sources have been scrutinized for potential conversion into bio-jet fuel, including sunflower oil [6], soybean oil [7], jatropha oil [8], refined palm kernel oil [9], *Calophyllum inophyllum* L. oil [10], and used palm cooking oil

* Corresponding author.
Email: karnawijaya@ugm.ac.id
https://doi.org/10.21924/cst.9.2.2024.1535

[11]. A pivotal criterion in selecting biomass as a feedstock for biofuel production is its non-edibility, ensuring it does not compete with the human food chain. The use of non-edible biomass sources, such as used vegetable oil, presents a sustainable and ethical solution to the biofuel production dilemma. Utilizing used vegetable oil, such as palm or coconut oil, not only addresses waste management concerns but also ensures that biofuel production does not compromise food security. Research indicates that used coconut cooking oil can be catalytically converted into biodiesel over $SO_4/ZrO_2$ and $CaO/ZrO_2$ catalysts, with reported yields reaching 55.35% [12].

Given that the carbon atom chain length of hydrocarbons constituting jet fuel falls within the $C_8$–$C_{16}$ range, used coconut cooking oil emerges as a promising candidate for bio-jet fuel production with high yield through hydrodeoxygenation and/or hydrocracking reactions. Sriatun et al. [13] reported the results of fresh coconut oil hydrocracking into bio-jet fuel with the NiO/ZTPA catalyst, with liquid product and selectivity of 60.07% and 34.10%, respectively. However, using fresh coconut cooking oil interferes with its functionality as a food for human consumption. This promising potential of used coconut cooking oil as a bio-jet fuel feedstock offers hope for sustainable solutions in the aviation industry.

This study undertook the hydrotreatment process of used coconut cooking oil utilizing a mordenite catalyst impregnated with cobalt metal (Co). Mordenite, a zeolite type with a Secondary Building Unit (SBU) 5-1 cage structure encompassing two primary channels, is favored for its large pore size, high surface area, thermal and mechanical stability, and rapid reactant diffusion rate [14–16]. However, employing mordenite alone as a hydrotreatment catalyst presents limitations in activity, selectivity, and stability, necessitating the dispersion of transition metal onto it. In this study, cobalt metal was chosen for its ability to enhance the catalytic performance of mordenite. The dispersion of cobalt metal onto mordenite was done to improve accessibility to the active site during the catalytic process, thereby enhancing the efficiency of the hydrotreatment process [17].

A previous study by Trisunaryanti et al. [15] reported the performance of the molybdenum-impregnated mordenite (15-Mo/Mor) catalyst on the conversion of refined palm kernel oil into bio-jet fuel, achieving a bio-jet fuel yield of 43.19%. Another report by Trisunaryanti and co-workers [18] demonstrated the successful application of a double-layer Ni/ZSM-5 catalyst in hydrotreating palm oil into bio-jet fuel, with a bio-jet fuel yield of 24.34%. However, it is important to note that using refined palm kernel oil and palm oil as feed is not sustainable due to their potential for human use, raising significant concerns about the future of bio-jet fuel production.

Cobalt is one such transition metal that enhances mordenite's catalytic performance in bio-jet fuel production. Its inclusion improves the selectivity of the desired hydrocarbon product due to the high affinity in the C–C bond breaking while reducing coke formation [19]. The spray impregnation method was chosen for dispersing cobalt metal due to its efficacy in minimizing solvent usage. It achieves a more uniform metal distribution on the support material than conventional wet impregnation, as reported by Triyono et al. [20]. They highlight the superiority of spray impregnation over wet impregnation in terms of total bio-hydrocarbon production and reduced oxygenated compound formation when adding cobalt metal to the Parangtritis beach sand matrix. Similarly, studies by Gao et al. [21] indicate that this method enhances the distribution of metal active sites on the support material surface, leading to increased dispersion. The findings of this study not only contribute to understanding the potential of used coconut cooking oil as a bio-jet fuel feedstock but also propose the Co/mordenite catalyst as a game-changer in the bio-jet fuel industry. This catalyst could significantly advance efforts to mitigate carbon emissions and support sustainable objectives, potentially revolutionizing the way we produce bio-jet fuel.

## 2. Materials and Methods

### *2.1. Materials*

The materials used in this study were mordenite purchased from Tosoh Corporation Japan, cobalt (II) chloride hexahydrate ($CoCl_2 \cdot 6H_2O$) purchased from Merck, deionized water supplied from CV Bima Aksara Nusa, nitrogen gas ($N_2$) and hydrogen gas ($H_2$) supplied from PT Surya Indotim Imex. Used coconut cooking oil as feed for bio-jet fuel production was obtained from a household in Sleman, Yogyakarta. Standard jet fuel was obtained from PT Pertamina.

### *2.2. Synthesis of the Co/mordenite catalyst*

Mordenite as catalyst support was first calcined at 500 °C with $N_2$ gas flowing at 20 mL/min for 4 h. The Co/mordenite catalyst was synthesized using the spray impregnation method. In a spray bottle, a 2% (wt%) cobalt (II) chloride hexahydrate was dissolved in 5 mL of deionized water. Then, the cobalt metal solution was sprayed on 5 g of calcined mordenite, and the mixture was mixed with a spatula at a constant speed for 30 seconds per spray. The mixture of the metal solution with the paste-formed mordenite was then dried in an oven at 120 °C for 60 min. The dried solid was then calcined at 500 °C with an $N_2$ gas flow rate of 20 mL/min for 4 h and then reduced at the same temperature with an $H_2$ gas flow rate of 20 mL/min for 4 h.

### *2.3. Characterization of the catalysts*

The crystallinity of the catalysts was determined by X-ray Diffractometer (XRD, SmartLab Rigaku) at 2θ of 5–85°. Fourier Transform Infrared spectrometer (FTIR, Shimadzu model Prestige-21) scanned at wavenumber of 400–4000 $cm^{-1}$ was used to identify the functional groups in the catalyst material. The acidity value of the catalyst was determined by Temperature-Programmed Desorption of Ammonia ($NH_3$-TPD, Micromeritrics Chemisorb 2750) with pre-treatment of the sample heated at 350 °C for 60 min under inert conditions (He gas) and $NH_3$ adsorption was carried out at 100 °C for 30 min followed by desorption at 100–800 °C. The textural properties of the catalysts were analyzed by Surface Area Analyzer (SAA, Micromeritics Gemini VII Version 5.03) with pre-treatment of the samples at a degassing temperature of 300 °C for 4 h. Surface morphology and elemental content were determined using Field Emission Scanning Electron Microscope with Energy Dispersive X-ray Spectrometer Mapping (FESEM-EDX Mapping, JEOL JSM-6510LA) and

Transmission Electron Microscope (TEM, JEM-1400 JEOL/EO). X-ray Photoelectron Spectrometer (XPS, Kratos Axis Supra Plus) was used to identify the composition of cobalt metal state in the catalyst. The thermal stability of the catalyst was determined using a Thermogravimetric/Differential Thermal Analyzer (TG/DTA, 5500 TA Instrument).

### *2.4. Hydrotreatment of used coconut cooking oil into bio-jet fuel*

Mordenite and cobalt-impregnated mordenite catalysts were tested for their catalytic performance in the hydrotreatment of used coconut cooking oil using a semi-batch reactor, i.e. upper furnace for catalyst and lower furnace for feed (see Fig. 1). The vaporized feed molecules from the lower furnace will move and contact the catalyst in the upper furnace. The hydrotreatment process was carried out at temperatures of 350–450 °C (fraction I) and 450–550 °C (fraction II) at atmospheric pressure for 2 h with a $H_2$ gas flow rate of 20 mL/min and a catalyst-to-feed ratio of 1:200 (w/w). The liquid product obtained was collected and analyzed by Gas Chromatography-Mass Spectrometer (GC-MS, Shimadzu QP2010S) using an EI 70 Ev ionizer and DB-5MS column to determine the catalyst selectivity to bio-jet fuel. Conversion of liquid, coke, and gas products can be calculated by Eqs. (1)–(3).

$$\text{Liquid product (wt\%)} = \frac{W_L(g)}{W_F(g)} \times 100\% \quad (1)$$

$$\text{Coke (wt\%)} = \frac{C_f(g) - C_i(g)}{W_F(g)} \times 100\% \quad 2)$$

$$\text{Gas product (wt\%)} = \frac{W_F(g) - W_L(g) - (C_f(g) - C_i(g))}{W_F(g)} \times 100\% \quad (3)$$

Where $W_F$ = weight of feed, $W_L$ = weight of liquid product, $C_f$ = weight of catalyst final, and $C_i$ = weight of catalyst initial. The selectivity and yield of bio-jet fuel were determined by Eqs. (4)–(5).

$$\text{Bio} - \text{jet fuel selectivity (\%)} = \frac{\text{GC–MS fraction area of } C_8 - C_{16}(\%)}{\text{total GC–MS area(\%)}} \times 100\% \quad (4)$$

$$\text{Bio} - \text{jet fuel yield (wt\%)} = \frac{\text{GC–MS fraction area of } C_8 - C_{16}(\%)}{\text{total GC–MS area(\%)}} \times \text{Liquid product (wt\%)} \quad (5)$$

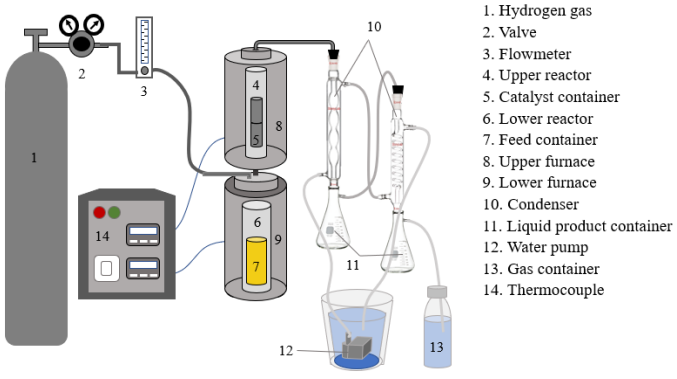


Fig. 1. Scheme of hydrotreatment reactor

## 3. Results and Discussion

### *3.1. Crystallinity of the catalysts*

Table 1. Degree of crystallinity of the catalysts

| Catalyst | Degree of crystallinity (%) |
|---|---|
| Mordenite | 68.45 |
| Co/mordenite | 56.57 |

Fig. 2 presents the XRD diffractograms of the mordenite and Co/mordenite catalysts. According to ICDD No 006-0239, the characteristic peaks for mordenite are identified at 2θ values of 9.76, 13.57, 15.35, 19.66, 22.44, 25.75, 27.67, and 30.97°, which are evident in all samples. Following the addition of cobalt onto mordenite, the X-ray diffractogram did not reveal the appearance of any new significant peaks. Only $Co_3O_4$ (311) crystals were detected at a 2θ value of 36.90°. This observation can be attributed to the low concentration of cobalt loading at merely 2% (wt%). The lack of significant alterations in the crystal structure of mordenite also suggests that cobalt is dispersed at a high degree of uniformity, with the crystal structure of mordenite being well preserved during the cobalt deposition [22]. However, as noted in Table 1, the Co/mordenite catalyst exhibits a lower degree of crystallinity compared to mordenite. This decrease in crystallinity may result from the loaded metal covering the pores of mordenite, leading to a reduction in the intensity of several sharp crystalline peaks associated with mordenite [15].

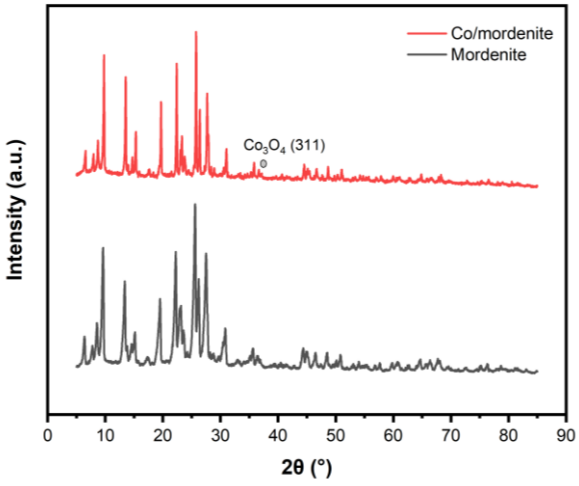


Fig. 2. X-ray diffractograms of the catalysts

### *3.2. FTIR analysis*

FTIR analysis was conducted to examine the functional groups present in the catalyst materials, and the resultant spectra are displayed in Fig. 3. The peak observed at a wavenumber of 1080 $cm^{-1}$ indicates the asymmetric stretching vibration of the T–O–T bond framework (T = Si or Al) within the mordenite structure. In contrast, the symmetric stretching vibration of the T–O–T bond framework is evidenced by the peak at a wavenumber of 810 $cm^{-1}$ [23]. The peak in the range of 447–563 $cm^{-1}$ corresponds to the bending vibration of the T–O–T bond framework [24]. Furthermore, the presence of peaks at wavenumbers 3426–3449 $cm^{-1}$ and 1620 $cm^{-1}$, attributed to

the stretching and bending vibrations of the –OH group, respectively, confirms the existence of –OH groups on the catalyst materials, which may derive from adsorbed $H_2O$ molecules or the presence of silanol and aluminol groups within the mordenite framework. Fig. 3 illustrates that the impregnation of cobalt onto mordenite does not induce the formation of new functional groups, indicating that the overall structure of mordenite remains unchanged.

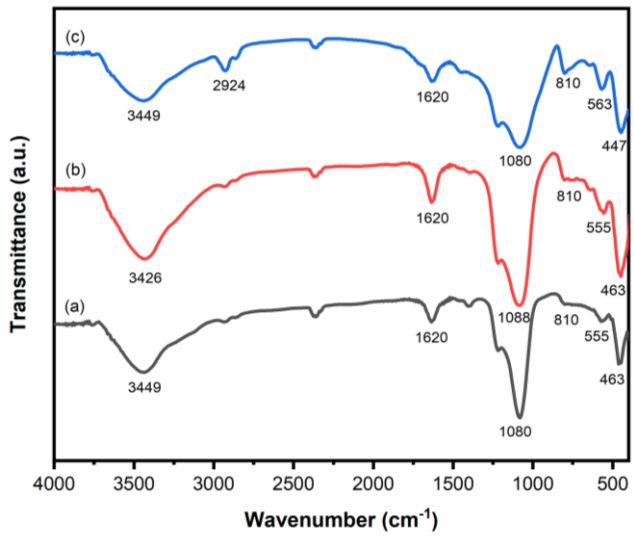


Fig. 3. FTIR spectra of (a) mordenite, (b) Co/mordenite fresh, and (c) Co/mordenite spent

### 3.3. Acidity study

The $NH_3$-TPD curves for the mordenite and Co/mordenite catalysts are presented in Fig. 4. Both curves exhibit two desorption peaks, where the desorption peak within the temperature range of 100–350 °C corresponds to weak acid sites, while strong acid sites are indicated by the desorption peak occurring between 350–800 °C. As summarized in Table 2, the dispersion of cobalt metal results in an increase in weak acidity while concurrently decreasing the strong acidity of mordenite. Consequently, the total acidity of the Co/mordenite sample is marginally lower than that of the mordenite sample. This observation may be explained by the interaction of cobalt metal species with Brønsted acid sites, which diminishes the proportion of $H^+$ ions present in the mordenite structure. Similar findings were reported by Sharifi et al. [25], who noted that the introduction of Mo metal into H-ZSM-5 led to a decrease in Brønsted acid sites and an increase in Lewis acid sites. Typically, Brønsted acid sites are prevalent at higher temperatures, while Lewis acid sites are found at lower temperatures. Cobalt possesses unoccupied 4p orbitals that can function as Lewis acid sites by accepting electron pairs from other species. These Lewis acid sites are later utilized to abstract hydride ions during the hydrotreatment process, facilitating the formation of carbenium ions that initiate the hydrocracking reaction.

### 3.4. Textural properties analysis

Fig. 5 illustrates the $N_2$ adsorption-desorption isotherm curves for the mordenite and Co/mordenite catalysts. Both samples display type IV adsorption-desorption isotherm curves, which, according to IUPAC classification, categorizes them as mesoporous materials (2 < pore diameter < 50 nm) [26]. The adsorption-desorption isotherm curves also exhibit a type H4 hysteresis loop, which characterizes the filling of micropores, corresponding to increased adsorption at low $P/P_0$ [27]. The pore geometry associated with this type of hysteresis is indicative of slit-shaped pores. In Fig. 5, it is evident that the quantity of $N_2$ adsorbed by the Co/mordenite sample is lower than that of mordenite, suggesting a decrease in the specific surface area and total pore volume of mordenite following the incorporation of cobalt metal.

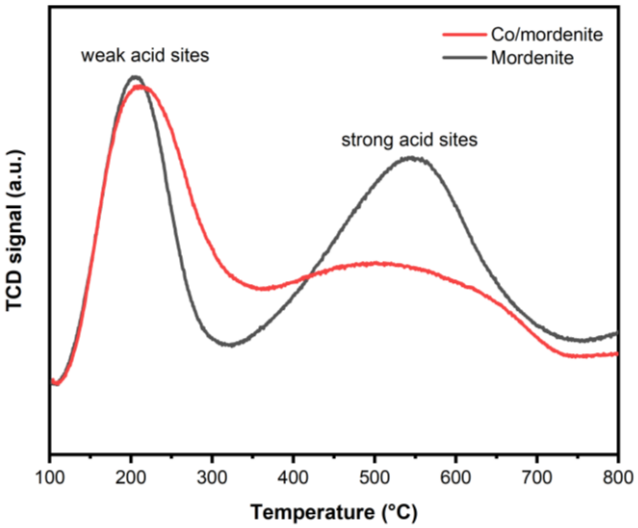


Fig. 4. $NH_3$-TPD curves of the catalysts

Table 2. Acidity of the catalysts obtained by $NH_3$-TPD

| Catalyst | Weak acidity (mmol/g) | Strong acidity (mmol/g) | Total acidity (mmol/g) |
|---|---|---|---|
| Mordenite | 0.777 | 1.220 | 1.997 |
| Co/mordenite | 0.998 | 0.755 | 1.753 |

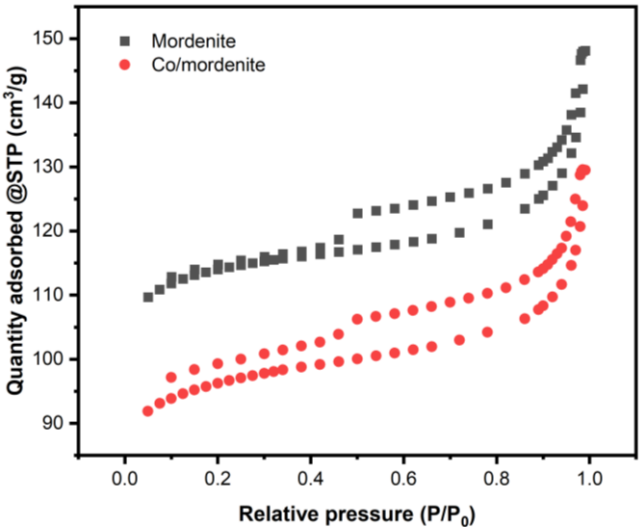


Fig. 5. $N_2$ adsorption-desorption curves of the catalysts

This statement is supported by the results of the textural properties analysis of the catalysts, employing the Brunauer-

Emmett-Teller (BET) and Barrett-Joyner-Halenda (BJH) equations, as summarized in Table 3. Mordenite possesses micro- and mesopore systems, with micropore volume predominating over mesopore volume. The pore size distribution curves for both samples, presented in Fig. 6, indicate that both samples are primarily characterized by pores with diameters of less than 2 nm. The incorporation of cobalt metal onto mordenite resulted in lower values for specific surface area, total pore volume, average pore diameter, and micropore volume compared to mordenite alone. This phenomenon may be attributed to the obstruction of mordenite pores by cobalt metal, consistent with the observed decrease in crystallinity from the XRD analysis results in Table 1. Meanwhile, the mesopore volume of the Co/mordenite increased slightly, suggesting that the presence of cobalt metal on the surface of the support material disrupts its textural properties.

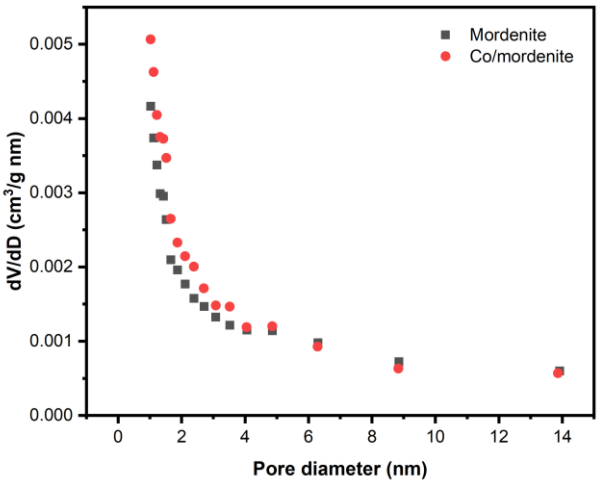


Fig. 6. Pore size distribution curves of the catalysts

Table 3. Textural properties of the catalysts

| Catalyst | Specific surface area ($m^2/g$) | Total pore volume ($cm^3/g$) | Average pore diameter (nm) | Micropore volume ($cm^3/g$) | Mesopore volume ($cm^3/g$) |
|---|---|---|---|---|---|
| Mordenite | 328.76 | 0.227 | 3.51 | 0.158 | 0.069 |
| Co/mordenite | 279.90 | 0.199 | 3.17 | 0.128 | 0.071 |

*3.5. Study of morphology and elemental composition of the catalysts*

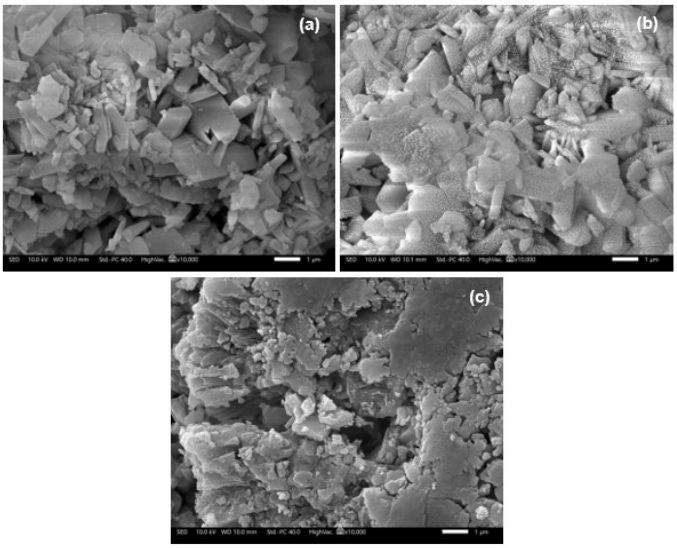


Fig. 7. FESEM micrographs of (a) mordenite, (b) Co/mordenite fresh, and (c) Co/mordenite spent at 10,000× magnification

The morphology of the catalyst materials was examined through the FESEM images presented in Fig. 7. Mordenite, as shown in Fig. 7(a), appears as a crystalline material characterized by an irregular flaky shape, non-uniform size, and smooth surface. Fig. 7(b) reveals that cobalt metal, introduced via spray impregnation, is successfully dispersed on the mordenite surface. In certain areas, the mordenite surface appears to be covered by smaller particles. The presence of 5.71% cobalt (see Table 4), as identified in the mapping image in Fig. 8, shows a reasonably uniform distribution at the sample test points.

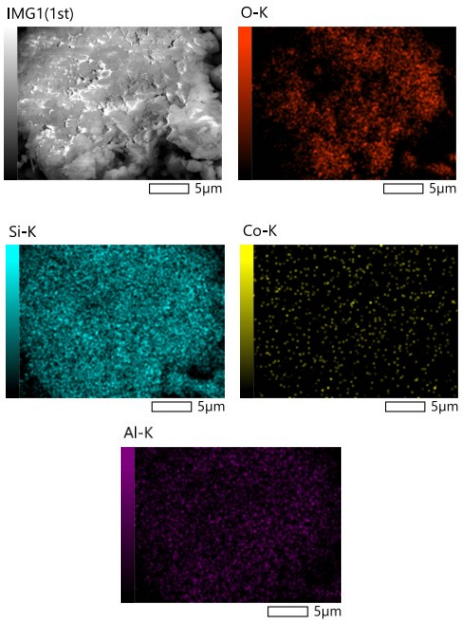


Fig. 8. Elemental mapping images of Co/mordenite fresh

TEM analysis, depicted in Fig. 9, further corroborates the observations regarding the morphology of the catalyst material and the positioning of the metal on the support material. Mordenite exhibits a porous structure, indicated by bright white spheres on the dark crystalline aggregates. As illustrated in Fig. 9(a), tiny particles of cobalt metal are observed within the pores of mordenite. This suggests that cobalt metal is not only dispersed on the surface of mordenite but also occupies its

pores, in accordance with the data showing a decrease in total pore volume and average pore diameter of mordenite.

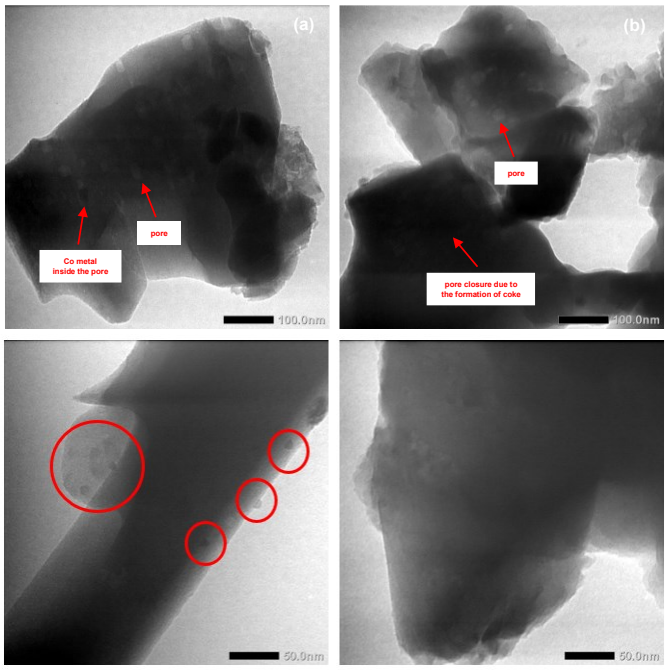


Fig. 9. TEM micrographs of (a) Co/mordenite fresh and (b) Co/mordenite spent at 100.0 nm (up) and 50.0 nm (down) magnification

Table 4. Elemental composition of the catalysts obtained by EDX

| Catalyst | Elemental content (wt%) | | | | |
|---|---|---|---|---|---|
| | Si | O | Al | Co | C |
| Mordenite | 47.07 | 48.27 | 4.66 | ND | ND |
| Co/mordenite fresh | 46.39 | 44.07 | 3.83 | 5.71 | ND |
| Co/mordenite spent | 34.73 | 35.73 | 2.81 | 2.97 | 23.76 |

ND = not detected

### 3.6. XPS analysis

XPS analysis was conducted to evaluate the state of metal elements on the catalyst, as the activity of the catalyst in the hydrotreatment process is primarily determined by the role of metal as the catalyst's active site. The XPS spectra of deconvoluted elemental cobalt are presented in Fig. 10. The deconvoluted Co XPS spectra reveal the oxidation states of elemental cobalt at 0 (Co), +2 (CoO), and +3 (in the form of $Co_3O_4$), with respective compositions of 3.6%, 51.7%, and 13.4%. The Co $2p_{1/2}$ peaks for each oxide are observed at binding energy values of 797.69 eV, 794.52 eV, and 792.01 eV, respectively. Conversely, the Co $_3p_{1/2}$ peaks for each oxidation state are located at binding energy values of 782.90 eV, 779.73 eV, and 778.14 eV, respectively [28,29]. In all oxidation states (0, +2, or +3), cobalt metal possesses a 3d orbital containing a single electron capable of homolytically dissociating hydrogen during hydrotreatment. Given its highest composition, the hydrotreatment process in this study was predominantly influenced by the presence of $Co^{2+}$. Ardini et al. [30] reported that $Co^{2+}$, as a CoO species distributed on $\gamma$-$Al_2O_3$ with Mo metal as a promoter (denoted as Co-Mo/$\gamma$-$Al_2O_3$ 24H), plays a significant role in hydrodeoxygenation and/or hydrocracking of used coconut oil into bio-hydrocarbons (85.61% biogasoline and 8.92% biodiesel).

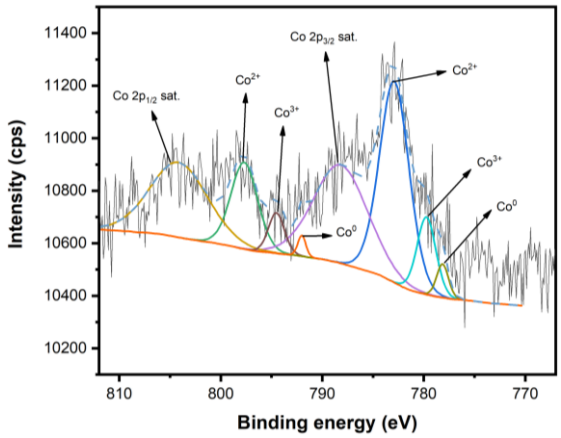


Fig. 10. Deconvoluted-XPS narrow scan spectra of cobalt metal of the Co/mordenite catalyst

### 3.7. TG/DTA analysis

The thermal stability of the Co/mordenite catalyst was investigated using a TG/DTA instrument. Fig. 11 presents the TG/DTA curves, indicating weight loss for the Co/mordenite samples over two temperature ranges. The Co/mordenite catalyst exhibited a weight loss of 11.23% at a temperature range of 0–200 °C, attributed to the release of water molecules adsorbed on the catalyst. Additionally, at a temperature range of 200–700 °C, the catalyst experienced a weight loss of 11.85% due to the release of hydroxyl groups bound strongly to the silanol or aluminol groups of mordenite [31].

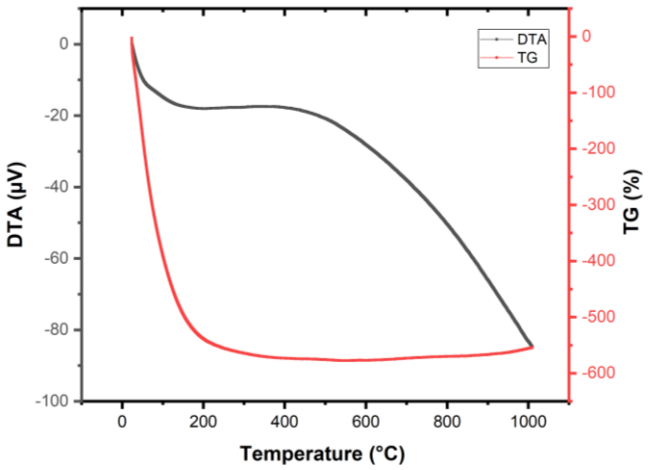


Fig. 11. TG/DTA profiles of the Co/mordenite catalyst

### 3.8. Conversion of used coconut cooking oil into bio-jet fuel over the catalysts

Used coconut cooking oil contains fatty acids ranging from $C_6$ to $C_{18}$, as shown in Table 5, with lauric acid comprising the highest content at 47.11%. These fatty acids undergo hydrodeoxygenation reactions to remove oxygen atoms and hydrocracking to break C–C bonds into jet fuel-range hydrocarbons ($C_8$–$C_{16}$).

During the hydrotreatment process, the feed is converted into three types of products: liquid products, coke (solid products), and gas products. The residue consists of unreacted feed remaining in the reactor. The product distribution from the hydrotreatment of used coconut cooking oil over the catalysts is displayed in a histogram in Fig. 12.

Table 5. Fatty acid composition in used coconut cooking oil obtained by GC-MS

| Fatty acid name | Chemical formula | Composition (%) |
|---|---|---|
| Caproic acid | $C_6H_{12}O_2$ | 0.40 |
| Caprylic acid | $C_8H_{16}O_2$ | 6.24 |
| Capric acid | $C_{10}H_{20}O_2$ | 5.87 |
| Lauric acid | $C_{12}H_{24}O_2$ | 47.11 |
| Myristic acid | $C_{14}H_{28}O_2$ | 17.78 |
| 9,12-Hexadecadienoic acid | $C_{16}H_{28}O_2$ | 2.37 |
| Palmitic acid | $C_{16}H_{32}O_2$ | 10.33 |
| 9-Octadecenoic acid | $C_{17}H_{32}O_2$ | 0.35 |
| 11-Octadecenoic acid | $C_{18}H_{34}O_2$ | 7.49 |
| Stearic acid | $C_{18}H_{36}O_2$ | 2.06 |

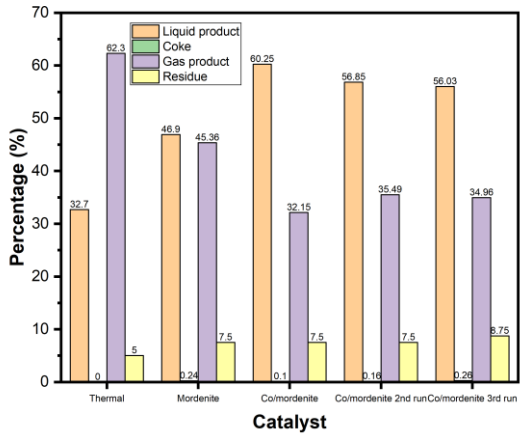


Fig. 12. Product distribution from hydrotreatment of used coconut cooking oil over the catalysts

As illustrated in Fig. 12, thermal hydrotreatment without a catalyst produced a higher gas product yield than catalytic hydrotreatment. In the reactor configuration applied in this study (see Fig. 1), the absence of a catalyst facilitates the movement of feed vapor, allowing heating treatment at high temperatures (up to 500 °C) to induce hydrocracking via a radical mechanism, resulting in dominant products in the form of gas-phase light-chain hydrocarbons [32]. Upon the addition of the catalyst, the hydrocracking reaction becomes more organized, enabling efficient contact between the vaporized feed and the active sites and pores of the catalyst, thus facilitating the formation of more liquid products as the desired output. Comparatively, when using mordenite alone without the incorporation of cobalt metal, the liquid product yield remains suboptimal, as the presence of cobalt metal enhances hydrodeoxygenation and/or hydrocracking reactions, increasing the frequency of collisions between the feed and $H_2$ gas. Consequently, the liquid product is generated more efficiently. Moreover, the dispersion of cobalt metal also reduces the amount of coke formed during the hydrotreatment process. The formation of coke poses a significant challenge to catalyst stability, as its deposition on the surface diminishes activity and selectivity.

The selectivity and yield of bio-jet fuel from the hydrotreatment of used coconut cooking oil are summarized in Table 6. This study separated the liquid product into two fractions, at temperatures of 350–450 °C (fraction I) and 450–550 °C (fraction II), to ascertain the optimal temperature for the hydrotreatment process. Thermal hydrotreatment yielded the lowest bio-jet fuel selectivity and yield compared to catalytic hydrotreatment. Consistent with previous discussions, the presence of a catalyst enhances selectivity towards the formation of the desired hydrocarbon fraction. Notably, the addition of 2% cobalt metal to mordenite via spray impregnation in this study resulted in a total bio-jet fuel yield of 51.11%, with the highest bio-jet fuel selectivity in fraction II reaching 88.90%.

Table 6. Bio-jet fuel selectivity and yield obtained from hydrotreatment of used coconut cooking oil

| Catalyst | Bio-jet fuel selectivity (%) | | Bio-jet fuel yield (wt%) | | Total bio-jet fuel yield (wt%) |
|---|---|---|---|---|---|
| | Fraction I* | Fraction II** | Fraction I* | Fraction II** | |
| Thermal | 49.65 | 57.69 | 5.89 | 11.62 | 17.51 |
| Mordenite | 64.79 | 76.13 | 10.88 | 22.91 | 33.79 |
| Co/mordenite fresh | 78.90 | 88.90 | 19.35 | 31.76 | 51.11 |
| Co/mordenite 2nd run | 76.57 | 83.10 | 17.23 | 28.54 | 45.77 |
| Co/mordenite 3rd run | 74.35 | 80.72 | 16.19 | 27.65 | 43.84 |

*350–450 °C

**450–550 °C

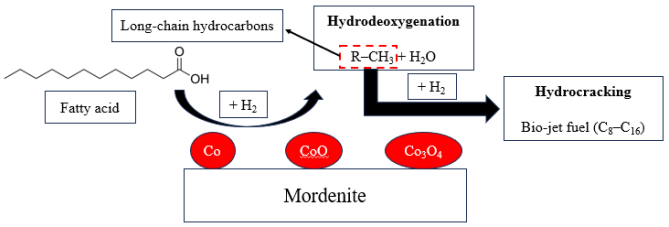


Fig. 13. Plausible reaction mechanism of bio-jet fuel production from used coconut cooking oil using the Co/mordenite catalyst

In addition to facilitating hydrocracking reactions, cobalt metal exhibits significant hydrodeoxygenation activity [33]. Cobalt-based catalysts demonstrate high selectivity for long-chain normal paraffins while reducing the proportion of oxygenated compounds, making them preferentially suitable for the production of synthetic biofuels [34]. A plausible reaction mechanism occurring during the hydrotreatment of used coconut cooking oil is depicted in Fig. 13. The fatty acids present in used coconut cooking oil predominantly fall within the jet fuel fraction range, with a minor proportion at $C_{18}$. Therefore, the conversion of this feed into bio-jet fuel necessitates limited hydrocracking reactions, while hydrodeoxygenation reactions should be maximized. This study observed that the impregnation of metal onto mordenite

effectively produced bio-jet fuel with a commendable yield, even under atmospheric pressure conditions.

### *3.9. Reusability test of the catalyst*

The reusability test for the Co/mordenite catalyst was conducted over three consecutive runs without any treatment prior to reuse. As shown in Fig. 12 and Table 6, a decline in liquid product, bio-jet fuel selectivity, and yield was noted following the catalyst's reuse. The results of the reusability test indicate that increased coke formation contributes to the deterioration of catalyst performance. Coke obstructs catalyst pores, hindering their accessibility for feed diffusion, thereby reducing the liquid product yield [10]. FESEM images in Fig. 7(c) and TEM images in Fig. 9(b) confirm the formation of coke, as the surface images of the material appear darker, indicating pore blockage by black clumps, identified as coke. EDX analysis in Table 4 and elemental mapping in Fig. 8 have successfully detected the presence of elemental carbon at 23.76% in the spent catalyst sample. Furthermore, the Co/mordenite spent sample (see Fig. 3(c)) displayed a peak at a wavenumber of 2924 $cm^{-1}$, corresponding to the vibration of $–CH_2–$ groups from the feed molecules. This observation confirms the occurrence of feed sequestration by the Co/mordenite catalyst during the hydrotreatment process [35].

### *3.10. Evaluation of liquid product from hydrotreatment over the Co/mordenite catalyst*

In the FTIR spectra (see Fig. 14), several characteristic absorption bands were observed, indicating the presence of various functional groups in the sample. The absorption band at 728 $cm^{-1}$ is attributed to the bending of $–(CH_2)n–$ groups. The band at 992 $cm^{-1}$ corresponds to the C–H bending of trans double bonds. The absorption at 1641 $cm^{-1}$ is associated with the vibration of the C=C group, while at 1713 $cm^{-1}$, the stretching of the –C=O group is noted. The peak at 2853 $cm^{-1}$ is due to symmetrical $–C–H(–CH_3)$ stretching, and the band at 2924 $cm^{-1}$ is attributed to asymmetrical $–C–H(–CH_3)$ stretching [36,37]. Fig. 14 illustrates a decrease in intensity of the carbon-oxygen bond vibrations, indicating the success of the hydrodeoxygenation reaction, alongside the formation of paraffin and olefin groups, thereby marking the completion of the hydrocracking reaction.

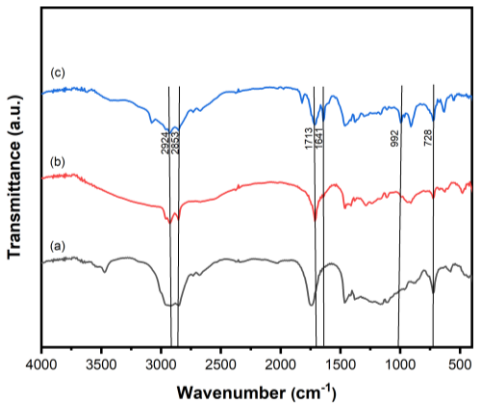


Fig. 14. FTIR spectra of (a) used coconut cooking oil, (b) liquid product fraction I, and (c) liquid product fraction II

Fig. 15 presents a compelling comparison of the number of carbon atoms in jet fuel range hydrocarbons between the liquid product of hydrotreatment (fraction II, exhibiting the highest selectivity) and standard jet fuel. Notably, hydrocarbons with $C_{10}$ chains dominate standard jet fuel, whereas our bio-jet fuel is characterized by a higher percentage of $C_{13}$ chains. Conversely, Fig. 16 displays the hydrocarbon group composition of the liquid product of hydrotreatment and standard jet fuel. Paraffins and olefins dominate our liquid product, while standard jet fuel contains a greater proportion of paraffins and iso-paraffins. These significant differences in carbon chain length and hydrocarbon group composition will undoubtedly result in distinct properties of the produced fuel.

The hydrotreatment process in this study, conducted at atmospheric pressure, offers a distinct advantage in alignment with the principles of green chemistry, thereby reducing costs and energy consumption. However, the process currently lacks the ability to saturate the obtained olefins into paraffins and to isomerize them into iso-paraffins. Consequently, further research is necessary to optimize all parameters and conduct additional tests, such as those for freezing point, flash point, boiling point, and others, to ensure that the produced bio-jet fuel meets ASTM specifications.

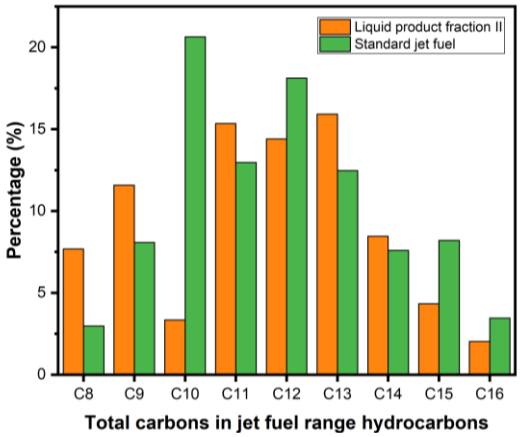


Fig. 15. Histogram of total carbons in jet fuel range hydrocarbons

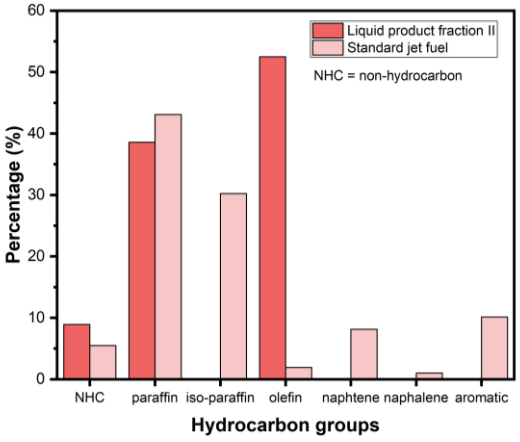


Fig. 16. Histogram of total carbons in jet fuel range hydrocarbons

## Conclusion

To sum up, fixing cobalt metal onto mordenite via spray

impregnation successfully modified its physicochemical properties. This alteration resulted in the development of the Co/mordenite catalyst with enhanced performance in converting used coconut cooking oil into bio-jet fuel, yielding a liquid product conversion and bio-jet fuel yield of 60.25% and 51.11%, respectively. The selectivity of bio-jet fuel in fractions I (350–450 °C) and II (450–550 °C) was 78.90% and 88.90%, respectively. The second and third applications of the Co/mordenite catalyst continued to produce commendable bio-jet fuel yields of 45.77% and 43.84%, respectively. Overall, this study provides an alternative pathway for producing bio-jet fuel by utilizing biomass-based waste from the hydrotreatment of used coconut cooking oil, thereby supporting the sustainable aviation industry. Nevertheless, numerous aspects warrant further exploration in future studies, including life-cycle analyses that encompass energy output-to-input ratios to assess the profitability of implementing this process on a large scale.

## Acknowledgements

This work was supported by the facilities from Physical Chemistry Laboratory, Department of Chemistry, Universitas Gadjah Mada. The authors are also grateful to the Radiation Laboratory Yogyakarta, the Advanced Physics Imaging Laboratories Serpong, and the Advanced Characterization Laboratories Serpong, National Research and Innovation Agency (BRIN) Indonesia.

## References

1. R. Tiwari, R. Mishra, A. Choubey, S. Kumar, A.E. Atabani, I.A. Badruddin, T.M.Y. Khan, *Environmental and economic issues for renewable production of bio-jet fuel: A global prospective*, Fuel 332 (2023) 125978.
2. S. Bhattacharjee, C.S. Tan, *Production of Biojet Fuel from Octadecane and Derivatives of Castor Oil Using a Bifunctional Catalyst Ni-Pd@Al-MCF in a Pressurized $CO_2$-Hexane-Water Solvent*, Energy & Fuels 36 (2022) 3119–3133.
3. J. Zhang, H. Fang, H. Wang, M. Jia, J. Wu, S. Fang, *Energy efficiency of airlines and its influencing factors: a comparison between China and the United States*, Resour. Conserv. Recycl. 125 (2017) 1–8.
4. S.S. Doliente, A. Narayan, J.F.D. Tapia, N.J. Samsatli, Y. Zhao, S. Samsatli, *Bio-aviation fuel: a comprehensive review and analysis of the supply chain components*, Front. Energy Res. 8 (2020) 1–38.
5. A. Zitouni, R. Bachir, W. Bendedouche, S. Bedrane, *Production of bio-jet fuel range hydrocarbons from catalytic HDO of biobased difurfurilydene acetone over Ni/$SiO_2$-$ZrO_2$ catalysts*, Fuel 297 (2021) 120783.
6. X. Zhao, L. Wei, J. Julson, Q. Qiao, A. Dubey, G. Anderson, *Catalytic cracking of non-edible sunflower oil over ZSM-5 for hydrocarbon bio-jet fuel*, New Biotech. 32 (2015) 300–312.
7. C.A. Scaldaferri, W.M.D. Pasa, *Production of jet fuel and green diesel range biohydrocarbons by hydroprocessing of soybean oil over niobium phosphate catalyst*, Fuel 245 (2019) 458–466.
8. I.H. Choi, J.S. Lee, C.U. Kim, T.W. Kim, K.Y. Lee, K.R. Hwang, *Production of bio-jet fuel range alkanes from catalytic deoxygenation of Jatropha fatty acids on a $WO_x$/Pt/$TiO_2$ catalyst*, Fuel 215 (2018) 675–685.
9. W. Trisunaryanti, K. Wijaya, I. Kartini, S. Purwono, Rodiansono, A. Mara, A.S. Rahma, *Hydrodeoxygenation of refined palm kernel oil (RPKO) into bio-jet fuel using Mo/H-ZSM-5 catalysts*, React. Kinet. Mech. Catal. 137 (2024) 843–878.
10. F. Visiamah, W. Trisunaryanti, Triyono, *Microwave-assisted coconut wood carbon-based catalyst impregnated by Ni and/or Pt for bio-jet fuel range hydrocarbons production from Calophyllum inophyllum L. oil using modified-microwave reactor*, Case Stud. Chem. Environ. Eng. 9 (2024) 1–12.
11. A.J. Saviola, K. Wijaya, A. Syoufian, W.D. Saputri, D.A. Saputra, I.T.A. Aziz, W.-C. Oh, *Hydroconversion of used palm cooking oil into bio-jet fuel over phosphoric acid-modified nano-zirconia catalyst*, Case Studies in Environ. Eng. 9 (2024) 100653.
12. E.P. Sari, K. Wijaya, W. Trisunaryanti, A. Syoufian, H. Hasanudin, W.D. Saputri, *The effective combination of zirconia superacid and zirconia-impregnated CaO in biodiesel manufacturing: Utilization of used coconut cooking oil (UCCO)*, Int. J. Energy Environ. Eng. 13 (2022) 967–978.
13. Sriatun, A. Darmawan, H. Susanto, Widayat, *The NiO and $MoO_3$ Enriched ZSM-5 as Catalyst for the Hydrocracking of Coconut Oil into Bio-jet Fraction*, Rasayan J. Chem. 15 (2022) 437–447.
14. S. Huang, X. Liu, L. Yu, S. Miao, Z. Liu, S. Zhang, S. Xie, L. Xu, *Preparation of hierarchical mordenite zeolites by sequential steaming-acid leaching-alkaline treatment*, Microporous Mesoporous Mater. 191 (2014) 18–26.
15. W. Trisunaryanti, Triyono, K. Wijaya, I. Kartini, S. Purwono, Rodiansono, A. Mara, A. Budiansyah, *Preparation of Mo-impregnated mordenite catalysts for the conversion of refined kernel palm oil into bioavtur*, Commun. Sci. Technol. 8 (2023) 226–234.
16. N. Gayathri, P. Tamizhdurai, C. Kavitha, V.L. Mangesh, P.S. Krishnan, A. Vijayaraj, R. Kumaran, N.S. Kumar, A.S. Al-Fatesh, S.B. Alreshaidan, *Fe-Ni bimetallic supported on mordenite catalyst for selective oxidation of veratryl alcohol in a continuous reactor*, Arabian J. Chem. 17 (2024) 105506.
17. A.N. Pulungan, R. Goei, F. Harahap, L. Simatupang, C. Suriani, S. Gea, M.I. Hasibuan, J.L. Sihombing, A.I.Y. Tok,. *Pyrolysis of Palm Fronds Waste into Bio-Oil and Upgrading Process Via Esterification-Hydrodeoxygenation Using Cu–Zn Metal Oxide Catalyst Loaded on Mordenite Zeolite*, Waste Biomass Valor. 15 (2024) 187–206.
18. W. Trisunaryanti, K. Wijaya, A.M. Tazkia, *Preparation of Ni/ZSM-5 and Mo/ZSM-5 catalysts for hydrotreating palm oil into biojet fuel*, Commun. Sci. Technol. 9 (2024) 161–169.
19. A. Yulianto, W. Trisunaryanti, T. Triyono, A.J. Saviola, K. Wijaya, I. Kartini, S. Purwono, R. Rodiansono, A. Mara, *Effect of arrangements in an atmospheric hydrotreating reactor of cobalt and/or molybdenum dispersed on activated carbon catalysts toward bio-jet fuel production from refined palm oil*, Case Studies in Environ. Eng. 10 (2024) 100894.
20. Triyono, W. Trisunaryanti, J. Purbonegoro, S.I. Aksanti, *Effect of cobalt impregnation methods on Parangtritis sand towards catalysts activity in hydrocracking of degummed low-quality Ujung Kulon Malapari oil into biohydrocarbons*, React. Kinet. Mech. Catal. 137 (2024) 303–321.
21. Y. Gao, W. Sun, W. Yang, Q. Li, *Creation of Pd/$Al_2O_3$ catalyst by a spray process for fixed bed reactors and its effective removal of aqueous bromate*, Sci. Rep. 7 (2017) 1–11.
22. M.T. Hapsari, W. Trisunaryanti, I.I. Falah, M.L. Permata, *Coating of Pd and Co on Mordenite for a Catalyst of Hydrotreating of Cashew Nut Shell Liquid into Biofuel*, Indones. J. Chem. 20 (2020) 1092–1100.
23. S.K. Saxena, N. Viswanadham, A.H. Al-Muhtaseb, *Enhanced selective oxidation of benzyl alcohol to benzaldehyde on mesopore created mordenite catalyst*, J Porous Mater. 23 (2016) 1671–1678.
24. W. Wangsa, A.J. Saviola, K. Wijaya, A. Bhagaskara, L. Hauli, D.A. Saputra DA, *Utilization of laboratory glove waste for fuel production through pyrolysis-hydrocracking consecutive process catalyzed by*

*sulfated Indonesian natural zeolite*, React. Kinet. Mech. Catal. 137 (2024) 1495–1514.

25. K. Sharifi, R. Halladj, S.J. Royaee, *An overview on the effects of metal promoters and acidity of ZSM-5 in performance of the aromatization of liquid hydrocarbons*, Rev. Adv. Mater. Sci. 59 (2020) 188–206.
26. M. Thommes K. Kaneko A.V. Neimark, J.P. Olivier, F. Rodriguez-reinoso, J. Rouquerol, K.S.W. Sing, *Physisorption of gases, with special reference to the evaluation of surface area and pore size distribution (IUPAC Technical Report)*, Pure Appl. Chem. 87 (2015) 1051–1069.
27. L. Xu, J. Zhang, J. Ding, T. Liu, G. Shi, X. Li, W. Dang, Y. Cheng, R. Guo, *Pore Structure and Fractal Characteristics of Different Shale Lithofacies in the Dalong Formation in the Western Area of the Lower Yangtze Platform*, Minerals 10 (2020) 72.
28. M.A. Ehsan, A.S. Hakeem, A. Rehman, *Hierarchical Growth of CoO Nanoflower Thin Films Influencing the Electrocatalytic Oxygen Evolution Reaction*, Electrocatalysis 11 (2020) 282–291.
29. S. Kalasina, K. Kongsawatvoragul, N. Phattharasupakun, P. Phattaraphuti M. Sawangphruk, *Cobalt oxysulphide/hydroxide nanosheets with dual properties based on electrochromism and a charge storage mechanism*, RSC Adv. 24 (2020) 14154.
30. M.A. Ardini, Triyono, T. Hara, N. Ichikuni, W. Trisunaryanti, *Study of metal sequenced spray impregnation method towards Co-Mo/γ-$Al_2O_3$ catalytic performance in hydrotreating of used coconut oil to liquid biohydrocarbon*, Microporous Mesoporous Mater. 382 (2025) 113357.
31. A.J. Saviola, K. Wijaya, W.D. Saputri, L. Hauli, A.K. Amin, H. Ismail, B. Budhijanto, W.-C. Oh, W. Wangsa, P. Prastyo, *Microwave-assisted green synthesis of nitrobenzene using sulfated natural zeolite as a potential solid acid catalyst*, Appl. Nanosci. 13 (2023) 6575–6589.
32. M. Utami, W. Trisunaryanti, K. Shida, M. Tsushida, H. Kawakita, K. Ohto, K. Wijaya, M. Tominaga, *Hydrothermal preparation of a platinum-loaded sulphated nanozirconia catalyst for the effective conversion of waste low density polyethylene into gasoline-range hydrocarbons*, RSC Adv. 9 (2019) 41392–41401.
33. A. Çakan, B. Kiren, N. Ayas, *Hydrodeoxygenation of safflower oil over cobalt-doped metal oxide catalysts for bio-aviation fuel production*, Mol. Catal. 546 (2023) 113219.
34. B.H.H. Goh, C.T. Chong, H.C. Ong, T. Seljak, T. Katrašnik, V. Józsa, J.-H. Ng, B. Tian, S. Karmarkar, V. Ashokkumar, *Recent advancements in catalytic conversion pathways for synthetic jet fuel produced from bioresources*, Energy Conv. Manag. 251 (2022) 114974.
35. W. Trisunaryanti, S. Larasati, S. Bahri, Y.L. Ni'mah, L. Efiyanti, K. Amri, R. Nuryanto, S.D. Sumbogo, *Performance comparison of Ni-Fe loaded on $NH_2$-functionalized mesoporous silica and beach sand in the hydrotreatment of waste palm cooking oil*, J. Environ. Chem. Eng. 8 (2022) 104477.
36. M.S.L. Ore, K. Wijaya, W. Trisunaryanti, W.D. Saputri, E. Heraldy, N.W. Yuwana, P.L. Hariani, A. Budiman, S. Sudiono, *The synthesis of $SO_4/ZrO_2$ and Zr/CaO catalysts via hydrothermal treatment and their application for conversion of low-grade coconut oil into biodiesel*, J. Environ. Chem. Eng. 8 (2020) 104205.
37. Amit, S. Kumari, R. Jamwal, *Use of FTIR spectroscopy integrated with multivariate chemometrics as a swift, and non-destructive technique to detect various adulterants in virgin coconut oil: a comprehensive review*, Food Chem. Adv. 2 (2023) 100203.